$E1$ strength in ^{208}Pb within the shell model

R. Schwengner,[1] R. Massarczyk,[1,2] B. A. Brown,[3] R. Beyer,[1] F. Dönau,[1] M. Erhard,[1,*] E. Grosse,[1,2] A. R. Junghans,[1] K. Kosev,[1] C. Nair,[1,†] G. Rusev,[1,‡] K. D. Schilling,[1] and A. Wagner[1]

[1]*Institut für Strahlenphysik, Forschungszentrum Dresden-Rossendorf, D-01314 Dresden, Germany*

[2]*Institut für Kern- und Teilchenphysik, Technische Universität Dresden, D-01062 Dresden, Germany*

[3]*National Superconducting Cyclotron Laboratory, Michigan State University, East Lansing, Michigan 48824, USA*

(Received 9 March 2010; revised manuscript received 6 April 2010; published 21 May 2010)

The dipole response of the doubly magic nuclide ^{208}Pb was studied in photon-scattering experiments at the electron linear accelerator ELBE with bremsstrahlung produced at kinetic electron energies of 9.0 and 15.0 MeV. The present (γ,γ') data combined with (γ,n) data from the literature are compared with results of shell-model calculations and calculations using a quasiparticle random-phase approximation. The shell-model calculations including (2p-2h) excitations describe the experimental $E1$ strength well and reproduce the spreading of the giant dipole resonance by applying a small smearing width only.

DOI: 10.1103/PhysRevC.81.054315 PACS number(s): 21.10.Tg, 21.60.−n, 23.20.−g, 27.80.+w

I. INTRODUCTION

The low-lying dipole strength as well as the isovector giant dipole resonance (GDR) in nuclei have attracted interest already for a long time. The dipole strength distribution and the related photoabsorption cross section σ_γ determine the reaction rates of photonuclear reactions such as photodisintegration reactions and the inverse reactions, for example, neutron capture. These reactions play an important role in specific processes of nucleosynthesis. Moreover, an improved experimental and theoretical description of neutron-capture reactions is of growing importance for next-generation nuclear technologies.

The GDR has been described by phenomenological approximations such as a Lorentz curve [1], later on extended by including an energy-dependent width [2,3] and phenomenological corrections for nuclear temperature [2–4] and for nuclear deformation [2,5]. These analytical approaches are currently available in databases for nuclear reactions [6] and are used in codes based on statistical reaction models [7,8]. A recent parametrization of the GDR by a combination of three Lorentzians with centroid energies according to a triaxially deformed oscillator [9] achieved an improved description of the GDR in deformed nuclei by using a spreading width depending only on the resonance energy as deduced from thermodynamical considerations [10].

Microscopic descriptions of the GDR are mainly based on the quasiparticle random-phase approximation (QRPA) that describes the coupling of two-quasiparticle ($2qp$) excitations and the formation of one-phonon modes. A problem of this approach is the strong fluctuations of the calculated electric dipole ($E1$) strength function that are at variance with the rather smooth behavior of the experimental data for the GDR. The observed spreading of the GDR has been explained as a collisional damping caused by higher order particle-hole excitations [11]. To simulate this spreading, an additional smearing is applied by folding the QRPA solutions with Lorentz curves of widths of about 3–4 MeV. Several attempts to improve the description have been made until now. An overview about these is given, for instance, in Ref. [12]. The residual couplings of quasiparticles to phonons neglected in the usual QRPA have been included, for example, in the quasiparticle-phonon model (QPM), applied to describe the low-lying strength below about 10 MeV so far [13], in the quasiparticle time-blocking approximation (QTBA) [14] or in the second random-phase approximation (SRPA) [15]. These models still require additional smearing to describe the spreading of the GDR. The extended theory of finite Fermi systems (ETFFS) based on QTBA calculations [16] provides an improved description of the spreading of the GDR. Moreover, the relativistic quasiparticle time-blocking approximation (RQTBA) [12,17], including spreading effects on the $4qp$ level in the fully consistent calculation scheme, reproduces the smooth behavior of the experimental data fairly well by applying small smearing widths of less than 500 keV. Because of the large numerical efforts, the preceding extensions of the QRPA models are restricted to spherical nuclei. Deformed nuclei were recently studied in a self-consistent QRPA with Skyrme interactions [18] and in a QRPA on the basis of a Woods-Saxon potential [19,20]. The latter has been extended by taking into account fluctuating shapes in slightly deformed transitional nuclei. This instantaneous-shape sampling [21] has improved the description of the experimental $E1$ strength but still requires additional smearing.

The $E1$ strength in the GDR region of the doubly magic ^{208}Pb has been used as a test for nearly all the approaches just mentioned. Calculations for ^{208}Pb are presented, for example, in Refs. [14,17,22–27]. In the present work, we test the predictions of the shell model for the $E1$ strength in ^{208}Pb. For this purpose, we revisit the low-lying dipole strength in ^{208}Pb by means of photon scattering and combine the present (γ,γ') data with (γ,n) data from literature. For comparison, results of a QRPA calculation are also presented.

*Present address: Istituto Nazionale di Fisica Nucleare, Sezione di Padova, I-35131 Padova, Italy.

†Present address: Argonne National Laboratory, Argonne, IL 60439, USA.

‡Present address: Department of Physics, Duke University, and Triangle Universities Nuclear Laboratory, Durham, NC 27708, USA.

 ©2010 The American Physical Society

II. EXPERIMENTAL METHODS AND RESULTS

We studied ^{208}Pb in a photon-scattering experiment using the bremsstrahlung facility [28] at the superconducting electron accelerator ELBE of the Forschungszentrum Dresden-Rossendorf. Bremsstrahlung was produced using electron beams of kinetic energies of 9.0 and 15.0 MeV with average currents of about 500 μA. The electron beams hit a radiator consisting of a niobium foil with a thickness of 7 μm.

The target was a disk with a diameter of 20 mm tilted by 45° on a horizontal axis perpendicular to the beam. The target mass was 2066.4 mg, enriched to 98.6% in ^{208}Pb. The lead disk was combined with 339.5 mg of ^{11}B, enriched to 99.5%, that was also shaped to a disk of 20 mm diameter to determine the photon flux from known scattering cross sections of levels in ^{11}B.

Scattered photons were measured with four high-purity germanium (HPGe) detectors of 100% efficiency relative to a 3 in. × 3 in. NaI detector. All HPGe detectors were surrounded by escape-suppression shields made of bismuth germanate (BGO) scintillation detectors. Two prevent γ rays scattered from surrounding materials from hitting the detectors, lead collimators of 10 cm thickness were placed in front of the detectors, and the BGO detectors were encased in cylindrically shaped lead layers of 2 cm thickness. Two HPGe detectors were placed vertically at 90° relative to the photon-beam direction at a distance of 28 cm from the target, resulting in opening angles of 16°. The other two HPGe detectors were positioned in a horizontal plane at 127° to the beam at a distance of 32 cm from the target with opening angles of 14°. The ratios of the γ-ray intensities measured at 90° and 127° were used to distinguish between dipole and quadrupole radiation. Absorbers of 20 mm Pb plus 3 mm Cu and of 8 mm Pb plus 3 mm Cu were placed in front of the detectors at 90° and 127°, respectively. Spectra of scattered photons were measured for 36 hours. Part of a spectrum including events measured at $E_e^{\rm kin} = 15.0$ MeV with the two detectors placed at 127° relative to the beam is shown in Fig. 1.

In photon-scattering experiments, the energy-integrated scattering cross section of an excited state can be deduced from the measured intensity of the respective transition to the ground state. The determination of the integrated scattering cross sections relative to the ones of states in ^{11}B has the advantage that the efficiencies of the detectors and the photon flux are needed in relative units only. We calculated the energy-dependent efficiencies for the four detectors by using GEANT4 [29]. The simulated efficiency curves were checked by using experimental efficiencies obtained from measurements with ^{22}Na, ^{60}Co, ^{133}Ba, and ^{137}Cs standard calibration sources. The bremsstrahlung spectrum was calculated by using a code [30] based on the approximation given in Ref. [31] and including a screening correction according to Ref. [32]. The calculated curve of the photon flux fits the experimental values derived from measured intensities, known integrated scattering cross sections [33,34] and angular distributions [35] of transitions in ^{11}B. For the calculated photon flux, we assumed an uncertainty of 6%, as obtained for the experimental relative flux derived from the 8913 keV transition in ^{11}B. Further details of the applied techniques are given in Refs. [36–40].

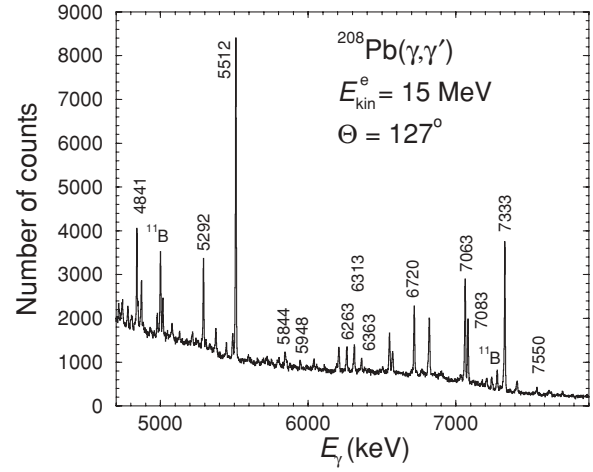

FIG. 1. Part of a spectrum of photons scattered from ^{208}Pb combined with ^{11}B, measured during the irradiation with bremsstrahlung produced by electrons of $E_e^{\rm kin} = 15.0$ MeV. This spectrum is the sum of the spectra measured with the two detectors placed at 127° relative to the beam. The most prominent peaks assigned to ground-state transitions from states in ^{208}Pb are marked with their energies in keV.

$J = 1$ states in ^{208}Pb with excitation energies from 4.8 to 8.0 MeV observed in each of the two experiments at $E_e^{\rm kin} = 9.0$ MeV and $E_e^{\rm kin} = 15.0$ MeV are presented in Table I. The given quantities were deduced from the experiment at 15.0 MeV and are consistent with the ones obtained at 9.0 MeV, which proves that the listed states are affected neither by feeding nor by neutron-induced reactions in the experiment at 15.0 MeV. In addition to the quantities deduced from the present experiments, we include the results of an earlier experiment with polarized photons at ELBE that is described in Ref. [28]. The relative nuclear self-absorption R in the target was determined according to Eq. (8.27) in Ref. [41]. The source energy spectrum $N(E)$ was assumed to be constant in the energy region around the resonance, as suggested in Ref. [41]. The areal density of nuclei deduced from target mass and geometry just described is $n_A d_A = 26.559 \times 10^{-6}$ fm^{-2}. The effective temperature $T_{\rm eff} = 302$ K was determined according to Eq. (8.19) in Ref. [41] by using the Debye temperature $\theta = 88$ K. Considering the target acting as absorber and as scatterer with on average equal contributions, half of the target thickness was used in the calculations, which corresponds to a first-order Taylor expansion of an exponential attenuation. The second order influences the result in the last digit only. For small partial level widths of $\Gamma_0 < 1$ eV, the calculated values of R come close to the ones obtained from the approximation of R given in Eq. (8.28) of Ref. [41] for the case $\Gamma_0 \ll E_\gamma \sqrt{2kT_{\rm eff}/Mc^2}$, where k is Boltzmann's constant and Mc^2 is the rest energy of the ^{208}Pb nucleus. In addition to the nuclear self-absorption, an electronic attenuation of 2% was taken into account. The resulting correction factors $C_{\rm sa} = 1 - R$ are given in Table I. These correction factors and the partial level widths listed in Table I were iteratively determined such that the partial level widths determined directly from measured intensities are reproduced after applying the given correction factors. Resonant self-absorption in the lead absorbers in front of the

TABLE I. $J = 1$ states from 4.8 to 7.6 MeV in ^{208}Pb.

E_x [a] (keV)	$\frac{I_\gamma(90^\circ)}{I_\gamma(127^\circ)}$ [b]	$\frac{I_{\gamma\parallel}-I_{\gamma\perp}}{I_{\gamma\parallel}+I_{\gamma\perp}}$ [c]	J_x^π [d]	I_s [e] (eVb)	Γ_0 [f] (eV)	C_{sa} [g]
4841.2(1)	0.90(8)	−0.33(3)	1^-	2174(250)	4.42(51)	0.81
5292.1(1)	0.75(6)	−0.33(3)	1^-	2382(273)	5.79(66)	0.83
5511.9(1)	0.79(7)	−0.32(2)	1^-	8455(979)	22.28(258)	0.88
5843.9(3)	1.3(3)	+0.18(10)	1^+	367(68)	1.09(20)	0.93
5947.6(4)	1.5(5)		1^-	226(57)	0.69(17)	0.95
6263.2(3)	0.72(8)	−0.23(8)	1^-	841(104)	2.86(36)	0.90
6312.9(1)	0.67(7)	−0.21(11)	1^-	1199(143)	4.14(49)	0.89
6362.7(3)	0.66(11)	−0.33(14)	1^-	430(60)	1.51(21)	0.93
6719.8(2)	0.75(7)	−0.22(3)	1^-	2746(317)	10.75(124)	0.88
7063.4(2)	0.78(7)	−0.22(2)	1^-	4373(509)	18.92(220)	0.90
7083.4(3)	0.70(7)	−0.19(3)	1^-	2476(296)	10.78(129)	0.89
7178.7(5)	1.3(3)		1	197(47)	0.88(21)	0.96
7206.1(5)	0.94(18)		1	114(36)	0.51(16)	0.96
7244.3(4)	0.83(18)		1 [h]	405(150)	1.84(68)	0.94
7280.5(6) [i]	0.6(3)		1^+	267(105)	1.23(48)	0.97
7332.6(2)	0.74(6)	−0.20(3)	1^-	7196(820)	33.56(383)	0.93
7549.6(3)	1.5(4)		1^-	196(41)	0.97(20)	0.96

[a]Excitation energy. The number in parentheses is the uncertainty in units of the last digit. This value was deduced from the γ-ray energy measured at 127° by including a recoil and Doppler-shift correction.

[b]Ratio of the intensities measured at angles of 90° and 127°. The expected values for an elastic pure dipole transition (spin sequence $0-1-0$) and for an elastic quadrupole transition (spin sequence $0-2-0$) are 0.74 and 2.15, respectively.

[c]Azimuthal asymmetry of the intensities deduced from the scattering of polarized photons. The values were taken from Ref. [28]. A negative value indicates $E1$ radiation; a positive value indicates $M1$ or $E2$ radiation.

[d]Spin and parity deduced from angular correlation and azimuthal asymmetry, respectively, of the ground-state transition. The values are consistent with the ones listed in Ref. [50] unless noted otherwise. The values in Ref. [50] were adopted if no or indefinite values were deduced from the present experiment, namely, for the states at 5843.9, 5947.6, 7178.7, and 7549.6 keV.

[e]Energy-integrated scattering cross section deduced from intensities measured at 127° and corrected for self-absorption (see text).

[f]Partial level width for the ground-state transition Γ_0. The branching ratio was assumed to be $\Gamma_0/\Gamma = 1$ according to Refs. [49,50]. The partial level width correlates with the integrated scattering cross section given in column 5 via the relation $I_s = g(\pi\hbar c/E_x)^2\Gamma_0^2/\Gamma$ with $g = (2J_x+1)/(2J_0+1)$.

[g]Correction factor for self-absorption (see text). The values of the integrated cross section and partial level width deduced from the measured intensity are reproduced when applying this factor to the respective values given in this table.

[h]In Ref. [50], the assignment 1^- is given for a state at 7240 keV found in (d, p) experiments.

[i]In Ref. [50], the assignment 1^+ is given for a state at 7278.7(2) keV. Angular correlation, integrated cross section, and partial level width were deduced from the experiment at $E_e^{\mathrm{kin}} = 9.0$ MeV, in which the target was not combined with ^{11}B.

detectors was neglected because the energies of the emitted γ rays are lowered due to recoil and Doppler shift by about 0.1–0.2 keV, whereas the level widths are smaller than about 0.02 keV.

The levels listed in Table I have been known from several earlier experiments [42–50]. However, the partial level widths of ground-state transitions given in those publications scatter over wide ranges, the largest values being by about 50% greater than the smallest ones for a given level. Moreover, most of the experiments do not cover the full energy range (see the compilations in Refs. [49,50]). The present work delivers partial level widths over the whole energy range up to the neutron-separation energy that have in several cases smaller uncertainties than those in previous work, and it confirms spin-parity assignments for several levels in an independent measurement. The level widths given in Table I may increase the confidence level of adopted values as generated in Ref. [50] from various experiments. We could not confirm the levels at 7415, 7631, 7685, 7723, and 7913 keV given in Refs. [48,50]. We observed transitions at 7415, 7631, 7646, 7723, and 7914 in the experiment at $E_e^{\mathrm{kin}} = 15.0$ MeV but not at $E_e^{\mathrm{kin}} = 9.0$ MeV, which may indicate their origin from neutron-induced reactions. Indeed, the doublet at 7631 and 7646 keV is known from the ^{56}Fe(n, γ) reaction [51].

The integrated scattering cross sections including the correction factors for self-absorption as given in Table I were used to derive absorption cross sections for energy bins of 200 keV. Our previous studies of dipole strength distributions in Mo isotopes and in $N = 50$ isotones have shown that up to about 70% of the dipole strength appear in a quasicontinuum of unresolved levels that is caused by the high level density at high excitation energy [20,36–39]. The comparison of the measured spectrum of ^{208}Pb with the simulated background caused by atomic processes in the lead target shows that only about 10% of the total strength in the energy range from 4.5 to 7.5 MeV can be ascribed to the quasicontinuum, which has been neglected.

The small contribution of the quasicontinuum in ^{208}Pb can be understood by considering level densities. The density of levels with spin $J = 1$ including both parities in the doubly magic nuclide ^{208}Pb amounts to 28/MeV at $E_x = 7$ MeV, for example, compared with 130/MeV in ^{92}Mo or 3290/MeV in ^{100}Mo according to the back-shifted Fermi gas model using the parameters given in Ref. [52]. In the following, we combine the photoabsorption cross sections derived from the present (γ,γ') data with cross sections of (γ,n) experiments covering the energy region of the GDR and compare them with the predictions of the shell model and also of QRPA calculations.

III. SHELL-MODEL CALCULATION OF THE $E1$ STRENGTH

The shell-model calculations for the $E1$ strength distribution in ^{208}Pb are based on the work in Ref. [53] for the double-octupole states in ^{208}Pb. The model space involves protons in the major shells $A = (1g_{7/2}, 2d_{5/2}, 2d_{3/2}, 3s_{1/2}, 1h_{11/2})$ and $B = (1h_{9/2}, 2f_{7/2}, 2f_{5/2}, 3p_{3/2}, 3p_{1/2}, 1i_{13/2})$, and neutrons in the major shells $C = (1h_{9/2}, 2f_{7/2}, 2f_{5/2}, 3p_{3/2}, 3p_{1/2}, 1i_{13/2})$ and $D = (1i_{11/2}, 2g_{9/2}, 2g_{7/2}, 3d_{5/2}, 3d_{3/2}, 4s_{1/2}, 1j_{15/2})$.

The simplest calculations assume a closed-shell (0p-0h) configuration for ^{208}Pb where the orbits in the A and C major shell are filled and those in the B and D major shells are empty. The 24 states involving the single-particle and the single-hole states in the surrounding nuclei (^{207}Pb, ^{209}Pb, ^{207}Tl, and ^{209}Bi) were then calculated and were used to set the single-particle energies of the Hamiltonian to those given in Fig. 1 of Ref. [54], which are based on the observed energies of the single-particle states in these nuclei. The energies of the unperturbed particle-hole energies and the corresponding $B(E1)$ values are those for pure proton or neutron excitations (with no center-of-mass correction for the $E1$ operator and spurious states not removed), shown for protons and neutrons in Fig. 2(a) and Fig. 2(b), respectively. The overall lower energy of neutron excitations reflects the smaller shell gap for neutrons compared to protons.

In the next step, the mixed (1p-1h) states in ^{208}Pb were calculated. [Note that these (1p-1h) states correspond to the elementary $2qp$ excitations in the QRPA and, accordingly, (2p-2h) states to $4qp$ excitations, etc.] The M3Y potential [55] was used for the particle-hole interactions. The two-body matrix elements (TBME) for the M3Y potential were calculated with harmonic-oscillator radial wave functions ($\hbar\omega = 6.88$ MeV). A center-of-mass Hamiltonian was employed to move the energy of the spurious 1^- state [a linear combination of (1p-1h) states] to a high excitation energy. This gave a low-lying collective 3^- state as well as many rather pure (1p-1h) states whose energies agree with those discussed in Ref. [54] to within an rms deviation of about 100 keV and whose dominating components also agree with the results of the reaction data discussed in Ref. [54]. In addition, the M3Y potential gives the collective $M1$ and $E1$ states at about their observed energies [56,57]. The $B(E1)$ distribution of the transitions from the (0p-0h) ground state to (1p-1h) states is shown in Figs. 2(c) and 2(d). The total $B(E1)$ strength is 99 e^2fm^2. For the $B(E1)$ values, no effective charges were used. When the isoscalar spurious state is removed, all the $E1$ matrix elements are purely isovector. In particular we note that most of the unperturbed single-particle strength that is clustered from 6 to 8 MeV is moved to a single state near 12 MeV (the isovector $E1$ resonance). In addition, we note that a few states are moved to a lower energy region around 4.5 MeV.

Our model space does not contain the highest energy part of the $E1$ strength distribution associated with the excitation of protons from the $1h_{11/2}$ orbit to the $1i_{11/2}$ and $2g_{9/2}$ orbits and neutrons from the $1i_{13/2}$ orbit to the $1j_{13/2}$ and $2h_{11/2}$ orbits. Thus, above 12 MeV, one should expect about 20% more $E1$ strength. This may also reduce the $E1$ strength at low energy.

The next step is to calculate the (2p-2h) states on top of and mixing with the (1p-1h) states. This was done starting with the M3Y interaction supplemented with the Kuo-Herrling renormalized G matrix [58] for the two-particle interaction involving the B and D major shells and the two-hole interaction involving the A and C major shells. In addition, the TBME for the Coulomb potential was calculated for the two proton major shells A and B. The single-particle energies were then readjusted to reproduce the energies given in Fig. 1 of Ref. [54] when the neighboring odd-even nuclei are calculated in a model space that includes an additional (1p-1h) excitation. For example, the model space for ^{207}Pb was $1h$ plus (1p-2h). All (2p-2h) states were shifted downward by 2.1 MeV to bring the energy of the monopole pairing vibration state close to its well-known experimental value of 4.86 MeV [59]. The justification for this shift in terms of the model-space truncation is discussed in Ref. [53].

The (0p-0h) $\rightarrow$ (1p-1h) + (2p-2h) $E1$ strength distribution is shown in Fig. 2(e). In comparison with the upper panels, one observes that the $B(E1)$ values and the level density below 8 MeV are dominated by the (1p-1h) spectrum. Above 8 MeV, there is a strong fragmentation of the strength into the (2p-2h) states. The total strength in this spectrum is the same as that in the (0p-0h) to (1p-1h) calculation (99 e^2 fm^2).

The (2p-2h) admixture in the ground state results in a ground-state wave function that includes only 66% of the closed-shell configuration. This describes the breaking of the closed shell in ^{208}Pb that is similar in size to that of nuclei such as ^{16}O [60] and ^{56}Ni [61] when considered in similar size model spaces. The ground-state energy is shifted down by about 11 MeV when (2p-2h) excitations are added. The $E1$ strength obtained in the model (0p-0h) + (2p-2h) $\rightarrow$ (1p-1h) + (2p-2h) (A) is shown in Fig. 2(f). The total strength in this calculation is reduced to 57 e^2 fm^2 due to the (2p-2h) ground-state correlations.

The (2p-2h) ground-state components can give additional strength going to (3p-3h) states that are not included in the present calculations. There are several aspects to consider. The full calculations would contain (0p-0h) + (2p-2h) $\rightarrow$ (1p-1h) + (2p-2h) + (3p-3h) (B). The (3p-3h) admixture into states that are predominantly (1p-1h) will reduce the (0p-0h) $\rightarrow$ (1p-1h) contribution in (B) compared to (A), but this reduction will be compensated by the additional (2p-2h) $\rightarrow$ (3p-3h) terms. The relatively pure (3p-3h) states start at about 15 MeV, with their collective strength pushed up to 20–30 MeV. These states can be reached from the (2p-2h) component of the ground state,

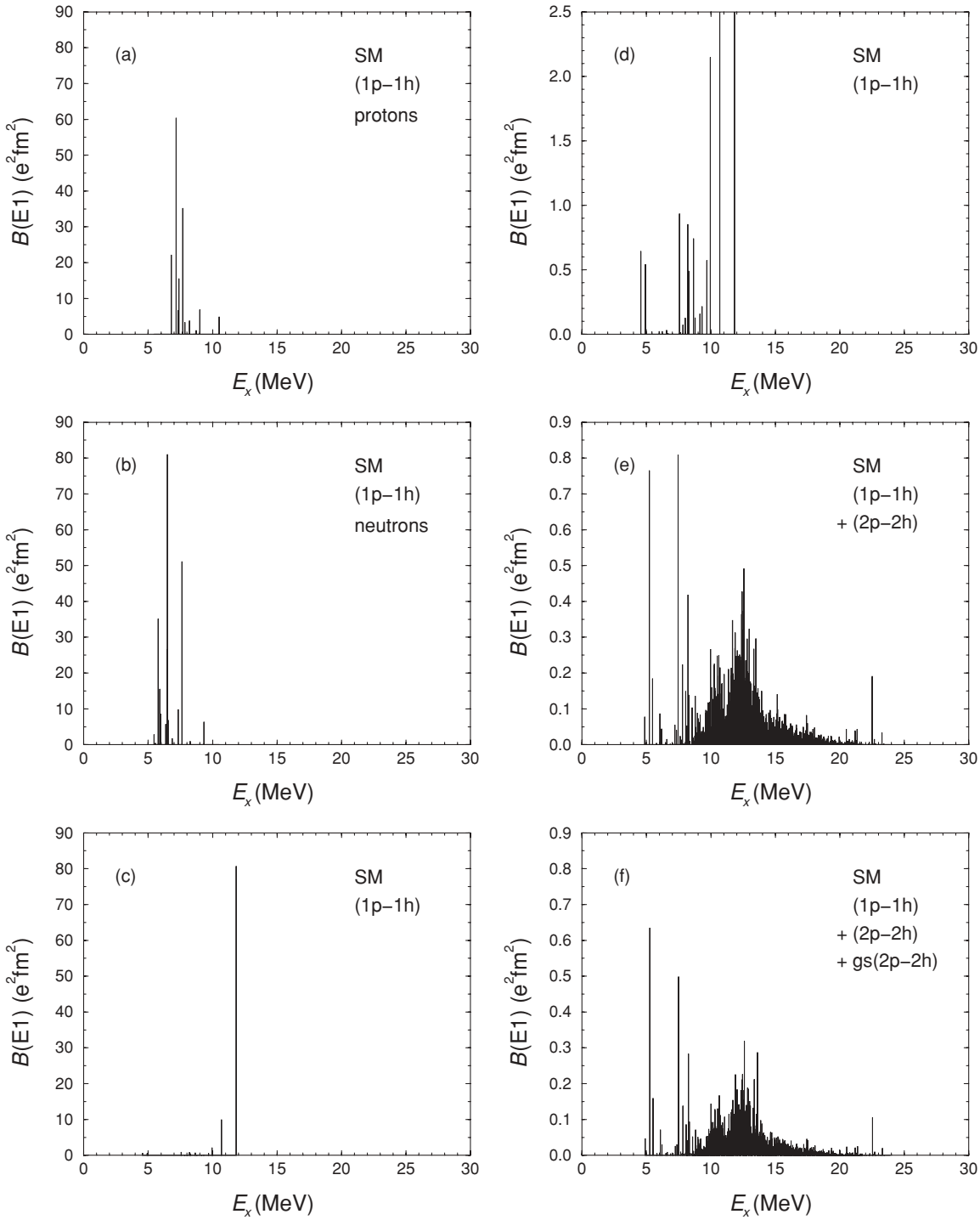

FIG. 2. Reduced $E1$ strengths for $0^+ \rightarrow 1^-$ transitions in ^{208}Pb resulting from the present shell-model calculations. (a, b) Pure (unmixed) (1p-1h) strengths for protons and neutrons, respectively. (c, d) Mixed (1p-1h) strength in different scales. Note that the dominating bars at about 11 and 12 MeV are cut in (d). (e) The (0p-0h) to (1p-1h) + (2p-2h) strengths. (f) Includes (2p-2h) admixtures to the ground state.

and this would give additional $E1$ strength above 15 MeV. The addition of (3p-3h) should be considered in future calculations.

IV. QRPA CALCULATION OF THE $E1$ STRENGTH

The general outline of the standard QRPA is presented in Refs. [62,63]. The present approach is based on an empirical Hamiltonian with separable dipole-plus-octupole interactions. The quasiparticle Hamiltonian consists of a Woods-Saxon mean field plus monopole pairing potential. The interaction terms comprise the isoscalar and isovector parts of the dipole-dipole and octupole-octupole interactions. The strength parameters of the repulsive isovector interaction were adjusted such that they reproduce the experimental maximum of the

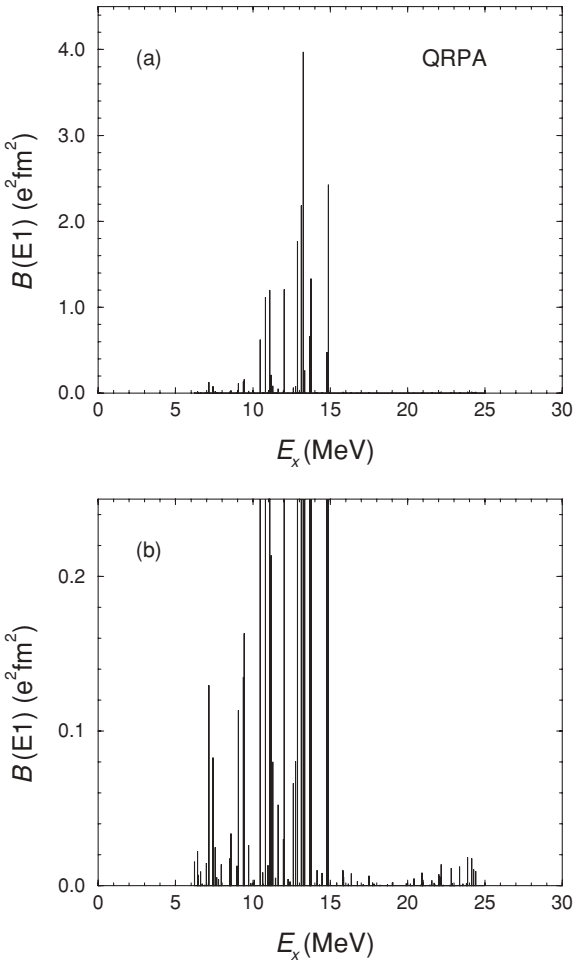

FIG. 3. Reduced $E1$ strengths for $0^+ \rightarrow 1^-$ transitions in ^{208}Pb resulting from the present QRPA calculations. (a, b) Strengths in different scales. Note that the dominating bars between 10 and 15 MeV are cut in (b).

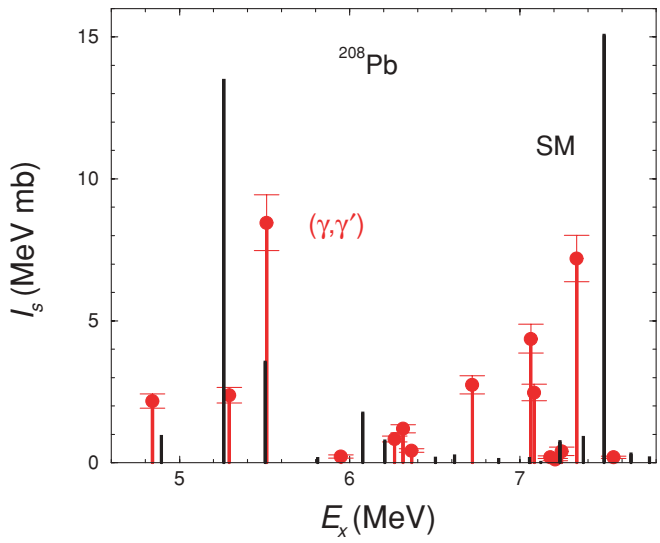

FIG. 4. (Color online) Experimental integrated scattering cross sections deduced from the present (γ,γ') experiments (red circles) compared with the ones deduced from the calculated $E1$ strengths shown in Fig. 2(f) (black bars).

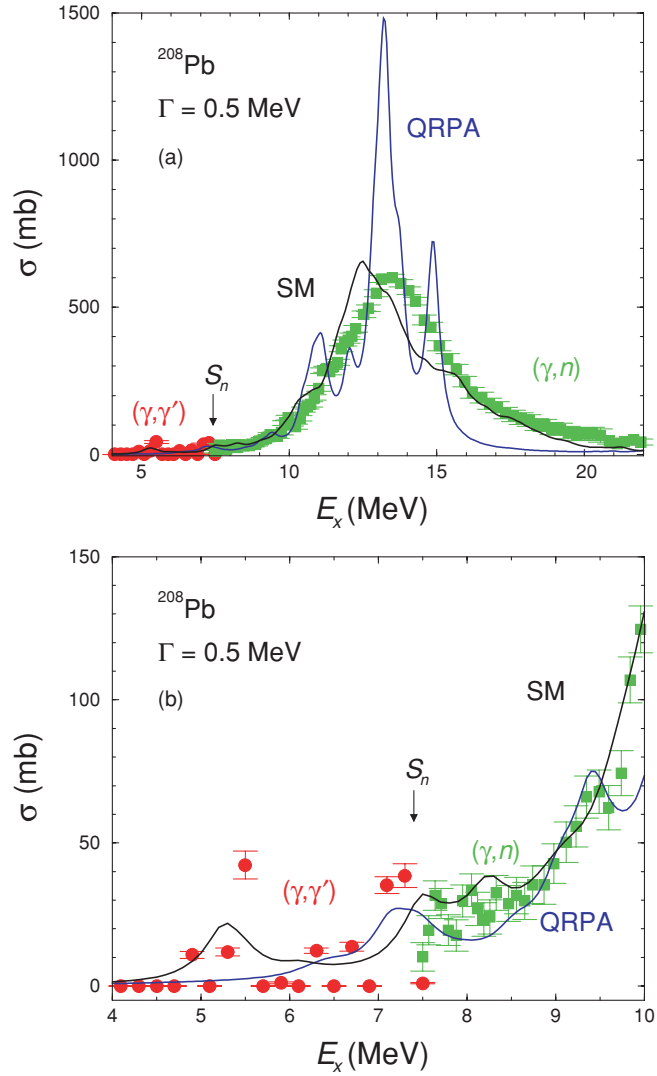

FIG. 5. (Color online) Experimental photoabsorption cross sections deduced from the present (γ,γ') experiments (red circles) and from (γ,n) experiments [67] (green squares) compared with the solutions of the shell-model calculations (black) and the QRPA calculations (blue), as shown in Figs. 2(f) and 3, respectively, but folded with Lorentz curves with a width of $\Gamma = 0.5$ MeV. (a) Energy region up to 22 MeV. (b) Zooms in on the low-energy part below 10 MeV. The neutron-separation energy of 7.4 MeV is marked S_n.

GDR. The suppression method described in Ref. [64] was applied to remove the effects of the spurious center-of-mass motion that may contaminate the calculated $E1$ strength. This method allowed us also to calculate the transition strengths without assuming any effective charge for the neutrons and using directly the bare proton charge e_π in the $E1$ transition operator. This model is described in detail in Ref. [19] and was applied in our recent studies of the $M1$ strength [65] and the $E1$ strength [20] in the series of even-mass Mo isotopes with $A = 92$–100 that imply spherical as well as deformed nuclear shapes. Besides, it was applied to describe the $E1$ strength in the nondeformed $N = 50$ isotones ^{88}Sr, ^{89}Y, and ^{90}Zr [39]. The $B(E1)$ strength in ^{208}Pb predicted by the present QRPA calculations is shown in Fig. 3.

V. COMPARISON OF MODEL PREDICTIONS WITH EXPERIMENTAL DATA

The experimental integrated cross sections given in Table I are compared with the ones predicted by the shell model in Fig. 4. The latter were deduced from the $B(E1)$ values shown in Fig. 2(f) according to the relation $I_s = \int \sigma_{\gamma\gamma} dE = 4.03 E_x B(E1, 0^+ \rightarrow 1^-)$ MeV mb, with E_x in MeV and $B(E1)$ in e^2 fm^2 [66]. As can be seen, the shell model predicts two states with strong cross sections at about 5.3 MeV and one state at about 7.5 MeV that are close to the strong experimental ones. These states include almost all strength in this energy region, whereas the experimental strength is somewhat more fragmented.

Absorption cross sections were deduced from the integrated scattering cross sections listed in Table I for energy bins of 200 keV width. These data from the present (γ,γ') experiment are combined with data from earlier (γ,n) experiments and are compared with the predictions of the shell-model calculations and the QRPA calculations in Fig. 5. The (γ,n) data were taken from Ref. [67] and scaled with a factor of 0.93 according to the findings of Ref. [68] for ^{197}Au and ^{208}Pb, which were recently confirmed in a photoactivation experiment for the case of ^{197}Au [69]. The solutions of the calculations were folded with Lorentz curves of widths of $\Gamma = 0.5$ MeV.

In the region of the GDR, the QRPA calculations show strong fluctuations and a large peak that exceeds the experimental maximum of the GDR by almost a factor 3. The folding with Lorentz curves of 0.5 MeV width is too small to smoothen the strengths of the few states visible in Fig. 3 such that they approach the experimental data. To smoothen these fluctuations sufficiently, greater widths of the Lorentz curves of about 3 MeV or more are needed. The curve resulting from the shell-model calculations is more smooth than the curve resulting from the QRPA calculations and hence is in much better agreement with the experimental data. The reason is that in contrast to the QRPA calculations, the shell-model calculations also include (2p-2h) excitations that lead to a strong fragmentation of the strength, in particular in the GDR region, as is seen already in Fig. 2(f).

We note that a good description of the spreading of the GDR is also achieved with RQTBA calculations accounting for (2p-2h) excitations [12,17]. This reflects that excitations of higher order than (1p-1h) are indeed the main mechanism for the spreading of the GDR, and their inclusion makes additional smearing superfluous.

VI. SUMMARY

We have revisited the low-lying $E1$ strength in the doubly magic nuclide ^{208}Pb in a photon-scattering experiment at the electron accelerator ELBE. The combination of these (γ,γ') data with (γ,n) data is compared with the predictions of the shell model and of QRPA. Whereas the QRPA cross sections still show large fluctuations when folding the solutions with Lorentz curves of a relatively small width of 0.5 MeV, the cross sections obtained from the shell model describe the behavior of the experimental values well. This is based on the inclusion of (2p-2h) excitations that cause a strong fragmentation of the strength and hence a spreading of the GDR.

ACKNOWLEDGMENTS

We gratefully acknowledge valuable discussions with E. Litvinova. We thank the staff of the ELBE accelerator for their cooperation during the experiments, and we thank GSI Darmstadt for the loan of the lead target. Support for this work was provided by the US National Science Foundation under Grant No. PHY-0758099.

[1] P. Axel, Phys. Rev. **126**, 671 (1962).
[2] S. G. Kadmenskii, V. P. Markushev, and V. I. Furman, Yad. Fiz. **37**, 277 (1983) [Sov. J. Nucl. Phys. **37**, 165 (1983)].
[3] J. Kopecky and M. Uhl, Phys. Rev. C **41**, 1941 (1990).
[4] Y. Alhassid and B. Bush, Nucl. Phys. A **509**, 461 (1990).
[5] F.-K. Thielemann and M. Arnould, in *Proceedings of the International Conference on Nuclear Data for Science and Technology*, edited by K. Blöckhoff (Reidel, Dordrecht, 1983), p. 762.
[6] T. Belgya *et al.*, IAEA Report No. TECDOC-1506, Vienna, 2006, [http://www-nds.iaea.org/RIPL-2/].
[7] T. Rauscher and F.-K. Thielemann, At. Data Nucl. Data Tables **75**, 1 (2000).
[8] A. J. Koning, S. Hilaire, and M. C. Duijvestijn, AIP Conf. Proc. **769**, 1154 (2005).
[9] A. R. Junghans, G. Rusev, R. Schwengner, A. Wagner, and E. Grosse, Phys. Lett. B **670**, 200 (2008).
[10] B. Bush and Y. Alhassid, Nucl. Phys. A **531**, 27 (1991).
[11] J. Wambach, Rep. Prog. Phys. **51**, 989 (1988).
[12] E. Litvinova, P. Ring, and V. Tselyaev, Phys. Rev. C **78**, 014312 (2008).
[13] N. Tsoneva and H. Lenske, Phys. Rev. C **77**, 024321 (2008).
[14] E. V. Litvinova and V. I. Tselyaev, Phys. Rev. C **75**, 054318 (2007).
[15] P. Papakonstantinou and R. Roth, Phys. Lett. B **671**, 356 (2009).
[16] A. Avdeenkov, F. Grümmer, S. Kamerdzhiev, S. Krewald, N. Lyutorovich, and J. Speth, Phys. Lett. B **653**, 196 (2007).
[17] E. Litvinova, P. Ring, and V. Tselyaev, Phys. Rev. C **75**, 064308 (2007).
[18] V. O. Nesterenko, W. Kleinig, J. Kvasil, P. Vesely, P.-G. Reinhard, and D. S. Dolci, Phys. Rev. C **74**, 064306 (2006).
[19] F. Dönau, G. Rusev, R. Schwengner, A. R. Junghans, K. D. Schilling, and A. Wagner, Phys. Rev. C **76**, 014317 (2007).
[20] G. Rusev *et al.*, Phys. Rev. C **79**, 061302(R) (2009).
[21] S. Q. Zhang, I. Bentley, S. Brant, F. Dönau, S. Frauendorf, B. Kämpfer, R. Schwengner, and A. Wagner, Phys. Rev. C **80**, 021307(R) (2009).
[22] D. Lacroix, S. Ayik, and P. Chomaz, Phys. Rev. C **63**, 064305 (2001).
[23] T. Nikšić, D. Vretenar, and P. Ring, Phys. Rev. C **66**, 064302 (2002).
[24] V. A. Rodin and M. H. Urin, Phys. Rev. C **66**, 064608 (2002).
[25] D. Sarchi, P. F. Bortignon, and G. Colò, Phys. Lett. B **601**, 27 (2004).

[26] S. Péru, J. F. Berger, and P. F. Bortignon, Eur. Phys. J. A **26**, 25 (2005).
[27] G. A. Lalazissis, T. Nikšić, D. Vretenar, and P. Ring, Phys. Rev. C **71**, 024312 (2005).
[28] R. Schwengner *et al.*, Nucl. Instrum. Methods A **555**, 211 (2005).
[29] S. Agostinelli *et al.*, Nucl. Instrum. Methods A **506**, 250 (2003).
[30] E. Haug, Radiat. Phys. Chem. **77**, 207 (2008).
[31] G. Roche, C. Ducos, and J. Proriol, Phys. Rev. A **5**, 2403 (1972).
[32] F. Salvat, J. D. Martinez, R. Mayol, and J. Parellada, Phys. Rev. A **36**, 467 (1987).
[33] R. Moreh, W. C. Sellyey, and R. Vodhanel, Phys. Rev. C **22**, 1820 (1980).
[34] F. Ajzenberg-Selove and J. H. Kelley, Nucl. Phys. A **506**, 1 (1990).
[35] G. Rusev, A. P. Tonchev, R. Schwengner, C. Sun, W. Tornow, and Y. K. Wu, Phys. Rev. C **79**, 047601 (2009).
[36] R. Schwengner *et al.*, Phys. Rev. C **76**, 034321 (2007).
[37] G. Rusev *et al.*, Phys. Rev. C **77**, 064321 (2008).
[38] R. Schwengner *et al.*, Phys. Rev. C **78**, 064314 (2008).
[39] N. Benouaret *et al.*, Phys. Rev. C **79**, 014303 (2009).
[40] R. Schwengner, A. Wagner, Y. Fujita, G. Rusev, M. Erhard, D. De Frenne, E. Grosse, A. R. Junghans, K. Kosev, and K. D. Schilling, Phys. Rev. C **79**, 037303 (2009).
[41] S. J. Skorka, in *The Electromagnetic Interaction in Nuclear Spectroscopy*, edited by W. D. Hamilton (North Holland, Amsterdam, 1975).
[42] C. P. Swann, Phys. Rev. Lett. **32**, 1449 (1974).
[43] D. F. Coope, L. E. Cannell, and M. K. Brussel, Phys. Rev. C **15**, 1977 (1977).
[44] R. M. Laszewski and P. Axel, Phys. Rev. C **19**, 342 (1979).
[45] T. Chapuran, R. Vodhanel, and M. K. Brussel, Phys. Rev. C **22**, 1420 (1980).
[46] K. Ackermann, K. Bangert, U. E. P. Berg, G. Junghans, R. K. M. Schneider, R. Stock, and K. Wienhard, Nucl. Phys. A **372**, 1 (1981).
[47] K. Wienhard, K. Ackermann, K. Bangert, U. E. P. Berg, C. Bläsing, W. Naatz, A. Ruckelshausen, D. Rück, R. K. M. Schneider, and R. Stock, Phys. Rev. Lett. **49**, 18 (1982).
[48] N. Ryezayeva, T. Hartmann, Y. Kalmykov, H. Lenske, P. von Neumann-Cosel, V. Y. Ponomarev, A. Richter, A. Shevchenko, S. Volz, and J. Wambach, Phys. Rev. Lett. **89**, 272502 (2002).
[49] J. Enders *et al.*, Nucl. Phys. A **724**, 243 (2003).
[50] M. J. Martin, Nucl. Data Sheets **108**, 1583 (2007).
[51] M. R. Bhat, Nucl. Data Sheets **85**, 415 (1998).
[52] T. von Egidy and D. Bucurescu, Phys. Rev. C **80**, 054310 (2009).
[53] B. A. Brown, Phys. Rev. Lett. **85**, 5300 (2000).
[54] M. Rejmund, M. Schramm, and K. H. Maier, Phys. Rev. C **59**, 2520 (1999).
[55] G. Bertsch, J. Borysowicz, H. McManus, and W. G. Love, Nucl. Phys. A **284**, 399 (1977).
[56] R. M. Laszewski, R. Alarcon, D. S. Dale, and S. D. Hoblit, Phys. Rev. Lett. **61**, 1710 (1988).
[57] N. Auerbach and B. A. Brown, Phys. Rev. C **60**, 025501 (1999).
[58] E. K. Warburton and B. A. Brown, Phys. Rev. C **43**, 602 (1991).
[59] G. Igo, P. D. Barnes, and E. R. Flynn, Ann. Phys. (NY) **66**, 60 (1971).
[60] E. K. Warburton, B. A. Brown, and D. J. Millener, Phys. Lett. B **293**, 7 (1992).
[61] T. Mizusaki, T. Otsuka, Y. Utsuno, M. Honma, and T. Sebe, Phys. Rev. C **59**, R1846 (1999).
[62] D. J. Rowe, in *Nuclear Collective Motion* (Methuen, London, 1970).
[63] P. Ring and P. Schuck, in *The Nuclear Many Body Problem* (Springer Verlag, Berlin, Heidelberg, 1980).
[64] F. Dönau, Phys. Rev. Lett. **94**, 092503 (2005).
[65] G. Rusev *et al.*, Phys. Rev. C **73**, 044308 (2006).
[66] A. Bohr and B. Mottelson, *Nuclear Structure II* (W. A. Benjamin, Inc., Reading, MA, 1975).
[67] A. Veyssiere, H. Beil, R. Bergere, P. Carlos, and A. Lepretre, Nucl. Phys. A **159**, 561 (1970).
[68] B. L. Berman, R. E. Pywell, S. S. Dietrich, M. N. Thompson, K. G. McNeill, and J. W. Jury, Phys. Rev. C **36**, 1286 (1987).
[69] C. Nair *et al.*, Phys. Rev. C **78**, 055802 (2008).